THE JOURNAL OF PHYSICAL CHEMISTRY C

Article

Cite This: J. Phys. Chem. C 2017, 121, 22644-22655

pubs.acs.org/JPCC

CO_2 Conversion in a Gliding Arc Plasmatron: Elucidating the Chemistry through Kinetic Modeling

Stijn Heijkers and Annemie Bogaerts*

Research Group PLASMANT, Department of Chemistry, University of Antwerp, Universiteitsplein 1, BE-2610 Wilrijk-Antwerp, Belgium

Supporting Information

ABSTRACT: By means of chemical kinetics modeling, it is possible to elucidate the main dissociation mechanisms of CO_2 in a gliding arc plasmatron (GAP). We obtain good agreement between the calculated and experimental conversions and energy efficiencies, indicating that the model can indeed be used to study the underlying mechanisms. The calculations predict that vibration-induced dissociation is the main dissociation mechanism of CO_2, but it occurs mainly from the lowest vibrational levels because of fast thermalization of the vibrational distribution. Based on these findings, we propose ideas for improving the performance of the GAP, but testing of these ideas in the simulations reveals that they do not always lead to significant enhancement, because of other side effects, thus illustrating the complexity of the process. Nevertheless, the model allows more insight into the underlying mechanisms to be obtained and limitations to be identified.

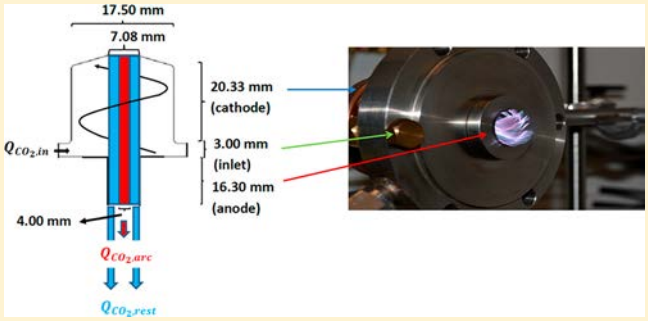

1. INTRODUCTION

The atmospheric CO_2 concentration has been increasing over the past two centuries from approximately 270 ppm to values exceeding 400 ppm, thus accelerating climate change.[1] Significant efforts need to be made to keep the increase in global average temperature well below 2 °C, as was agreed at the Paris climate conference (COP21).[2] Technologies for converting CO_2 into value-added products, such as fuels, are therefore highly desirable, as they can turn waste back into new feedstock, following the cradle-to-cradle principle.[3]

In recent years, there has been increasing interest in the use of plasmas for CO_2 conversion.[4−35] In addition to pure CO_2 splitting into CO and O_2,[5−24] reactions with CH_4 (i.e., dry reforming),[25−31] H_2O,[32] N_2,[33,34] and H_2[35] have also been studied. Most research is performed using dielectric barrier discharges (DBDs)[5−7,27−33] and microwave (MW) plasmas.[8−16,26,34] The highest energy efficiencies (>50% and even up to 90%) have been achieved using a microwave setup, and this is attributed to vibrational excitation, leading to dissociation of CO_2.[11−16] However, these highest energy efficiencies in microwave plasmas were obtained at reduced pressures, which is undesirable for industrial applications. DBDs, on the other hand, operate at atmospheric pressure, and they are already used in industry for ozone synthesis,[36] but their energy efficiency is more limited (typically up to 10%), because the CO_2 dissociation proceeds mainly through electronic excitation, which is less efficient.[16,4] The conversion and energy efficiency in a DBD can be improved by inserting a packing inside the plasma, but the energy efficiency remains limited.[31]

Another type of plasma has recently gained considerable interest for CO_2 conversion, namely, the so-called gliding arc (GA) discharge, which operates at atmospheric pressure and is clearly more efficient than the DBD, with reported efficiency values of about 25−29%.[18,19] A conventional GA discharge is formed between two flat diverging electrodes. The arc ignites at the shortest interelectrode distance and "glides" toward larger interelectrode distances by means of the gas flow, until it extinguishes and a new arc ignites again at the shortest distance, so that the cycle is repeated. However, because of the high current density of the discharge, conventional GA reactors suffer from electrode degradation. Moreover, a significant amount of gas does not pass through the active plasma (arc) region, so it will not be converted.[19,20] To tackle these issues, a new type of GA discharge, based on cylindrical electrodes and tangential gas inlets, was recently developed. It is also called a "gliding arc plasmatron" (GAP) and is based on vortex flow stabilization, that is, forward vortex flow (FVF) and/or reverse vortex flow (RVF) stabilization.[21,37,38] The highest energy efficiencies for CO_2 conversion have been obtained using the RVF configuration, because it is characterized by a secondary, backward-oriented inner vortex gas stream within the outer tangential gas flow, confining the plasma and resulting in nearly perfect heat insulation from the wall, better gas mixing with the arc, and therefore a higher conversion and energy efficiency.[21,23]

Received: July 3, 2017
Revised: September 18, 2017
Published: September 20, 2017

DOI: 10.1021/acs.jpcc.7b06524
J. Phys. Chem. C 2017, 121, 22644−22655

Table 1. Species Taken into Account in the 0D Model

molecules	charged species	radicals	excited species
CO_2, CO	CO_2^+, CO_4^+, CO^+, $C_2O_2^+$, $C_2O_3^+$, $C_2O_4^+$, C_2^+, C^+, CO_3^-, CO_4^-	C_2O, C, C_2	CO_2(Va, Vb, Vc, Vd), CO_2(V1−V21), CO_2(E1), CO(V1−V10), CO(E1−E4)
O_2, O_3	O^+, O_2^+, O_4^+, O^-, O_2^-, O_3^-, O_4^- electrons	O	O_2(V1−V3), O_2(E1, E2)

Some experimental work and fluid dynamics modeling have been performed for the GAP, to study the CO_2 conversion under different operating conditions[21,23,25] and to describe the typical gas flow and plasma characteristics in argon[24,38] and in CO_2.[24] However, to our knowledge, no detailed kinetic study has yet been performed to elucidate the main dissociation mechanisms of CO_2 in a GAP. Nevertheless, this information is crucial to obtain insight into the underlying chemistry in an effort to improve the process.

Therefore, in this article, we present a detailed study of the CO_2 conversion and energy efficiency in a GAP reactor, using zero-dimensional (0D) chemical kinetics modeling with a full description of the vibrational kinetics throughout the arc, validated by experiments. This allows us to elucidate the most important CO_2 dissociation mechanisms, and to identify the limitations, which can be helpful for further improving the performance of the GAP for energy-efficient CO_2 conversion.

2. MODEL DESCRIPTION

First, we provide a general description of the 0D model and the chemistry data set used in the simulations, followed by the assumptions in the 0D approach for describing the arc region in the GAP and the conditions used in the model.

2.1. 0D Model Equations. The 0D model is based on solving a set of conservation equations for all individual species included in the model

$$\frac{\partial n_s}{\partial t} = \sum_{i=1}^{j} [(a_{s,i}^{R} - a_{s,i}^{L})R_i] \quad (1)$$

where n_s is the density of species s (in m^{-3}); j is the total number of reactions; $a_{s,i}^{L}$ and $a_{s,i}^{R}$ are the stoichiometric coefficients at the left-hand side and right-hand side, respectively, of the reaction; and R_i is the rate of reaction (in m^{-3} s^{-1}), given by

$$R_i = k_i \prod_s n_s^{\alpha_{s,i}} \quad (2)$$

where k_i is the rate constant (in m^3 s^{-1} or m^6 s^{-1} for two-body or three-body reactions, respectively). In addition, the balance equation for the gas temperature T_g (in K) is also solved

$$N\frac{\gamma k}{\gamma - 1}\frac{dT_g}{dt} = P_{e,el} + \sum_j R_j \Delta H_j - P_{ext} \quad (3)$$

where $N = \sum n_i$ is the total neutral species density, γ is the specific heat ratio of the total gas mixture, k is the Boltzmann constant (in J K^{-1}), $P_{e,el}$ is the gas heating power density due to elastic electron−neutral collisions (in W m^{-3}), R_j is the rate of reaction j (in m^{-3} s^{-1}), ΔH_j is the heat released (or consumed when this value is negative) by reaction j (in J), and P_{ext} is the heat loss due to energy exchange with the surroundings (in W m^{-3}). More details about the model can be found in the Supporting Information.

2.2. Chemistry Data Set. The chemistry data set used in this study is based on the original model of Kozák and Bogaerts,[11] which was thoroughly reviewed by Koelman et al.[39] The electron-impact reaction rate constants are calculated using a pre-evaluated electron energy distribution function (EEDF, which is regularly updated during the simulations based on the new chemical composition in the plasma) and the cross-section data set of Phelps and co-workers with a 7 eV threshold excitation reaction used for dissociation,[40−42] as suggested by Grofulović et al.,[43] Bogaerts et al.,[44] and Pietanza et al.[45−47] The species described in the kinetic model are listed in Table 1.

The symbols V and E within parentheses for CO_2, CO, and O_2 represent the vibrationally and electronically excited levels, respectively, of these species. All 21 levels (V1−V21) of the asymmetric mode until the dissociation limit (5.5 eV) are taken into account, because they are crucial for storing vibrational energy for efficient CO_2 dissociation.[16] In addition, four effective low-lying symmetric stretching and bending mode levels are included in the model (Va−Vd). We take only one electronically excited level (E1), with an energy of 10.5 eV, into account, as the excitation level with an energy of 7 eV immediately gives rise to dissociation (see above).

A large number of reactions are taken into account, such as electron-impact reactions; electron−ion recombination reactions; and ion−ion, ion−neutral, and neutral−neutral reactions, as well as vibration−translation (VT) and vibration−vibration (VV) relaxation reactions. Furthermore, reactions considering carbon production are also included in the model. More information about the species and reactions included in the model can be found in the articles of Kozák and Bogaerts,[11] Koelman et al.,[39] and Bogaerts et al.[44]

2.3. Modeling the GAP Reactor with a 0D Approach. The GAP under study is based on the experimental design used by Ramakers et al.[23] and Nunnally and co-workers,[21,22] as illustrated in Figure 1. It is a cylindrical GA reactor in which the

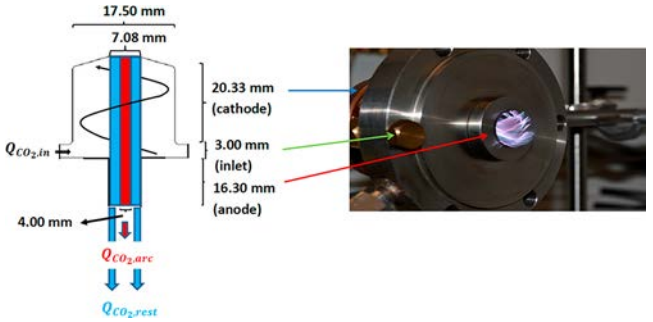

Figure 1. Schematic diagram of the GAP, with characteristic dimensions of the cathode (reactor body), inlet region (insulator), anode (outlet), and arc region and an indication of the outer vortex (solid spiral). The inner (reverse) vortex is not depicted for the sake of clarity, but it is confined within the red and blue rectangles. The red rectangle shows the arc region, as considered in the model. $Q_{CO_2,in}$, $Q_{CO_2,arc}$, and $Q_{CO_2,rest}$ denote the fluxes of CO_2 entering the reactor, leaving the arc, and leaving the rest of the reactor, respectively. (See text for more explanation.)

DOI: 10.1021/acs.jpcc.7b06524
J. Phys. Chem. C 2017, 121, 22644−22655

gas flow enters through a tangential inlet, resulting in a vortex flow. A potential difference is applied between the reactor body and the outlet of the reactor, which act as cathode and anode, respectively. This potential difference creates an arc between the cathode and the anode. When the anode diameter is smaller than the cathode diameter, the incoming gas will not immediately escape the reactor through the outlet at the bottom of the reactor, as it follows a vortex flow with a larger diameter, so it will be forced upward into the cathodic part of the reactor, in a so-called forward vortex flow (FVF) pattern. As a result of friction and inertia, the rotational speed will be reduced. Therefore, when the spiraling gas arrives at the top of the reactor, it will start to move downward in a smaller vortex, toward the outlet at the bottom, that is, in a reverse vortex flow (RVF). Because of this vortex flow, the arc plasma is stabilized in the center of the reactor, and the reverse vortex gas flow is forced through the plasma. This is schematically illustrated in Figure 1 and can be described by the fluid dynamics modeling of Trenchev and co-workers.[24,38]

The reactor body (or cathode) has a length of 20.3 mm and a diameter of 17.50 mm. Ramakers et al.[23] performed experiments with three grounded electrodes, acting as anode and outlet, with a constant length of 16.30 mm but different diameters, namely, 7.08, 14.30, and 17.50 mm. In our study, we focus on the anode with the smallest diameter, for which the RVF effect is most pronounced, so that this anode yields the highest conversion and energy efficiency, as explained in ref 23.

Combining a complete fluid dynamics and chemical kinetics description of CO_2 conversion in a GAP plasma with a two-dimensional (2D) or three-dimensional (3D) model is computationally not yet affordable, but because the plasma confined in the inner vortex is more or less uniform,[38] we assume a constant power density applied to the gas during its residence time in the plasma [i.e., when traveling in the inner (reverse) vortex]. Therefore, 0D modeling of this type of plasma is justified. Indeed, the species conservation equations (see eqs 1 above) solve for the species densities as functions of time, but the time dependence can be translated into a spatial dependence, that is, a function of position in the arc column, based on the gas velocity, because of the similarity between a batch reactor and a plug-flow reactor. The same method was also applied in our previous works (see refs 5, 11, 12, 15, 30, 32−34, and 48).

However, some assumptions need to be made, as follows:

(1) Trenchev et al.[38] and Ramakers et al.[23] revealed that the plasma density and the arc width do not change significantly with electrical current and gas flow rate, and thus, we employ a constant arc radius for all calculations. Based on 3D turbulent gas flow pattern calculations using the shear stress transport (SST) Reynolds-averaged Navier−Stokes (RANS) turbulent model,[49] in combination with a 3D fluid plasma model, as explained in ref 38, the actual arc in the GAP seems to have a radius of 1 mm. However, the temperature just outside the arc is still high enough to induce plasma and, therefore, CO_2 dissociation. Moreover, the 3D calculations were performed in argon, and CO_2 will be characterized by higher gas temperatures, because of the occurrence of VT relaxation, so the arc region in a CO_2 plasma will be wider. Finally, because of the skewed spiral motion of the arc, the actual volume covered by the arc will be somewhat larger than predicted by the 3D−2D fluid simulations. Therefore, we assume a constant arc radius of 2 mm, which, in combination with a total arc length of 39.6 mm (see Figure 1), results in a total plasma volume of 497.6 mm^3. Still, not all gas flowing in the reverse vortex, which has more or less the same radius as the outlet (i.e., 3.54 mm),[24] will be treated by the arc plasma. Therefore, further research will be needed to improve the gas inlet configuration and the reactor design, to enhance the amount of gas treated by the plasma.

(2) The initial gas temperature (i.e., right before entering the arc region) is set to room temperature (293.15 K). Inside the arc, the gas will quickly heat up. The actual gas temperature inside the arc is adopted from 3D fluid model calculations[24] and not calculated self-consistently in the present model. Indeed, the latter approach might be too much of an approximation, as it accounts only for gas heating due to collisions and chemical reactions and heat loss to the environment, but does not take into account turbulent heat losses, which have been reported to be important in the GAP.[24] However, the position in the arc at which this gas temperature is reached is determined by solving eq 3. As soon as this gas temperature is reached, the value is kept constant for the rest of the arc column (see below), based on ref 24.

(3) A constant mass flow rate through the reactor is assumed, and the pressure is held constant at atmospheric pressure, in agreement with the 3D fluid dynamics calculations of Trenchev et al.[24] Because the gas temperature will rise as a function of residence time (or position in the arc), the particle densities will decrease, to maintain constant pressure. Furthermore, the gas velocity will increase to conserve the mass flow rate. As the conservation equations for the various species (eqs 1) do not account for gas expansion at constant pressure, we calculate the gas pressure at every time step of the simulation from the actual species densities and gas temperature, and the species densities are then corrected to maintain a constant (atmospheric) pressure, following the approach of Kozák and Bogaerts.[12]

(4) The initial gas velocities in the arc region, at each gas flow rate considered in this study, are adopted from the 3D gas flow patterns calculated by the fluid dynamics model of ref 24. The corresponding velocities are 1.96, 2.55, 3.14, 3.72, and 4.31 m/s, for gas flow rates of 10, 13, 16, 19, and 22 L/min, respectively. These velocities are updated during each time step of the simulation, as described above, to maintain constant mass flow rate and pressure.

The CO_2 conversion after passing through the arc, $X_{CO_2,arc}$, is defined as

$$X_{CO_2,arc}\ (\%) = 100\%\left(1 - \frac{n_{CO_2,e} v_e}{n_{CO_2,i} v_i}\right) \quad (4)$$

where $n_{CO_2,e}$ and v_e are the CO_2 density (in m^{-3}) and gas velocity (in m s^{-1}), respectively, at the end of the arc region near the outlet and $n_{CO_2,i}$ and v_i are the CO_2 density (in m^{-3}) and gas velocity (in m s^{-1}), respectively, at the beginning, right before entering the arc region (i.e., at room temperature). Note that the same formula can be used to calculate the CO_2 conversion as a function of position in the arc, simply by using the CO_2 density and gas velocity at that position in the arc.

Because not all gas in the reactor passes through the arc region, the total CO_2 conversion in the reactor, which is also measured experimentally, will be lower than the CO_2 conversion after passing through the arc region, as it is also necessary to account for the unconverted CO_2 in the reactor. This total conversion, $X_{CO_2,tot}$, is defined as

DOI: 10.1021/acs.jpcc.7b06524
J. Phys. Chem. C 2017, 121, 22644−22655

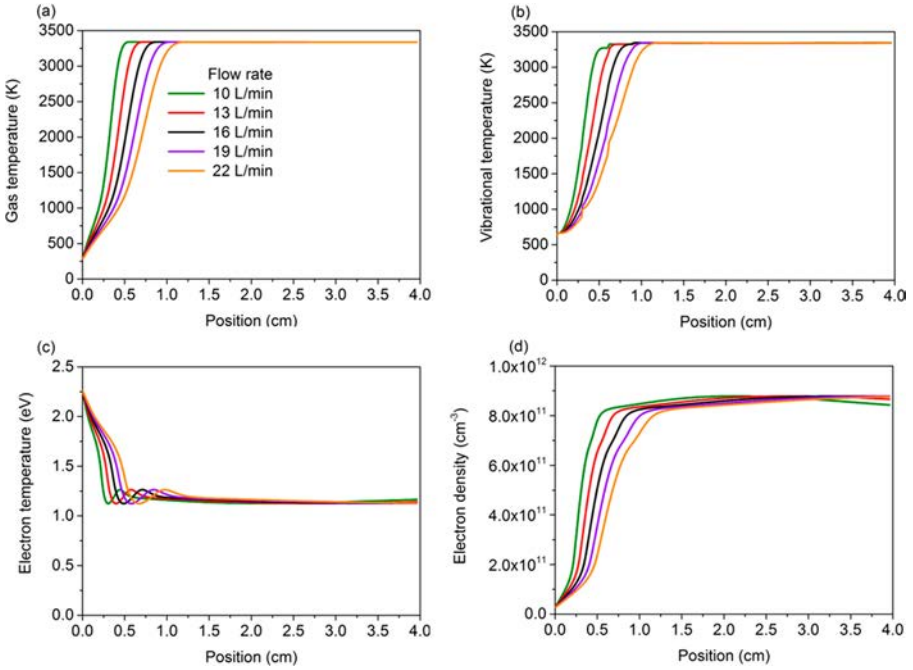

Figure 2. (a) Gas temperature, (b) vibrational temperature, (c) electron temperature, and (d) electron density as functions of the position in the arc column calculated for different gas flow rates at a plasma power of 650 W.

$$X_{CO_2,tot}\ (\%) = 100\%\left(1 - \frac{Q_{CO_2,arc} + Q_{CO_2,rest}}{Q_{CO_2,in}}\right) \quad (5)$$

where $Q_{CO_2,in}$, $Q_{CO_2,arc}$, and $Q_{CO_2,rest}$ are the CO_2 fluxes (in s^{-1}) entering the reactor, exiting the arc region at the outlet, and exiting the reactor without passing through the arc, hence without being converted, respectively. This means that the fraction of CO_2 that passes through the arc region must be defined, as explained below.

The CO_2 flux entering the reactor, $Q_{CO_2,in}$, is defined as

$$Q_{CO_2,in} = n_{CO_2,i}\dot{V} \quad (6)$$

where $n_{CO_2,i}$ is the CO_2 density (in m^{-3}) at the inlet of the reactor (at room temperature) and $\dot{V}$ is the volumetric flow rate (in $m^3\ s^{-1}$). The CO_2 flux exiting the arc region at the outlet $Q_{CO_2,arc}$ is defined as

$$Q_{CO_2,arc} = n_{CO_2,e}v_eA_{arc} \quad (7)$$

with $n_{CO_2,e}$ and v_e are the CO_2 density (in m^{-3}) and gas velocity (in m s^{-1}), respectively, at the end of the arc region near the outlet and A_{arc} is the cross-sectional area of the arc region (i.e., 12.57 mm^2). Finally, because of conservation of mass, the flux of CO_2 that is not treated by the plasma, $Q_{CO_2,rest}$, is given by

$$Q_{CO_2,rest} = Q_{CO_2,in} - n_{CO_2,i}v_iA_{arc} \quad (8)$$

Hence, the fraction of CO_2 that passes through the arc region is defined by the mass flow rate through the arc and is 14.8% of the total mass flow rate through the reactor. The remaining 85.2% does not pass through the arc and will not be converted.

The energy efficiency (E_{eff}) is defined as

$$E_{eff}\ (\%) = \frac{[X_{CO_2,tot}\ (\%)]\Delta H}{SEI} \quad (9)$$

where ΔH is the energy cost of splitting one CO_2 molecule into CO and $^1/_2O_2$ (i.e., 2.9 eV/molecule) and SEI is the specific energy input (in eV/molecule), which is calculated as

$$SEI = \frac{P_{plasma}k_BT_{gas,in}}{1.60 \times 10^{-19}p\dot{V}} \quad (10)$$

where P_{plasma} is the plasma power (in W), k_B is the Boltzmann constant (in J K^{-1}), $T_{gas,in}$ is the gas temperature at the reactor inlet (i.e., 293.15 K), p is the pressure (i.e., 1.01325×10^5 Pa), and $\dot{V}$ is the volumetric flow rate (in $m^3\ s^{-1}$). The conversion factor of 1.60×10^{-19} (J/eV) in the denominator is for changing from units of joules to electronvolts.

The vibrational temperature, T_v, is calculated from the densities of the various asymmetric-mode levels, assuming that they follow a Boltzmann distribution

$$T_v(K) = \frac{1}{i}\sum_{i=1}^{k}\frac{(-E_{i-1} + E_i) \times 11605}{\ln\left(\frac{n_i}{n_{i-1}}\right)} \quad (11)$$

where E_i and E_{i-1} are the energies (in eV) of the ith and $(i-1)$th asymmetric-mode levels, respectively, and n_i and n_{i-1} are the corresponding densities (in m^{-3}) of the ith and $(i-1)$th asymmetric-mode levels. The conversion factor of 11605 in the numerator is for changing from units of electronvolts to kelvin, and k is the number of asymmetric-mode levels taken into account, which follow a (quasi-) Boltzmann distribution. In the beginning of the arc column (i.e., first 0.30 cm), only the first asymmetric-mode level is taken into account ($k = 1$) in calculating the vibrational temperature, because the vibrational distribution function (VDF) does not exhibit a Boltzmann distribution for higher levels for all flow rates studied (see Figure S.1 of the Supporting Information). Between 0.30 and 0.60 cm, the first four asymmetric-mode levels are taken into account ($k = 4$); between 0.60 and 0.90 cm, the first seven asymmetric-mode levels are taken into account ($k = 7$); and after 0.90 cm, the first 10 asymmetric-mode levels ($k = 10$) are

DOI: 10.1021/acs.jpcc.7b06524
J. Phys. Chem. C 2017, 121, 22644−22655

taken into account, because they follow a Boltzmann distribution here (see Figure S.1 of the Supporting Information). The energies of the different vibrational levels included in the model are listed in Table S.1 of the Supporting Information.

3. RESULTS AND DISCUSSION

3.1. Plasma Characteristics Inside the Arc. To understand the CO_2 conversion in the GAP, it is necessary to first obtain a good insight into the main plasma characteristics defining the CO_2 conversion, namely, the gas temperature, vibrational temperature, electron temperature, and electron number density. These parameters are plotted as functions of position in the arc column in Figure 2 for different flow rates, ranging from 10 to 22 L/min (i.e., the same values as used in the experiments of ref 23). We used a plasma power of 650 W, lying somewhat in the middle of the experimental range (529−712 W) used in ref 23.

As is clear from Figure 2a, the gas temperature rises quickly until its maximum defined value of 3340 K. Although this gas temperature seems to be quite high, 3D−2D fluid simulations show that the arc temperature in CO_2 is about 3100 K for a plasma power of 500 W.[24] In this work, we consider a power of 650 W, so we assume a slightly higher gas temperature in the arc. Furthermore, the rotational/gas temperature in a similar setup was measured in ref 22, and values of 2700 ± 50 K were obtained for a CO_2 plasma doped with 1% N_2 for a plasma power of 200 W. Because our plasma power is more than 3 times higher, we believe that the assumption of an arc temperature of 3340 K is reasonable. Nevertheless, one must realize that this is only an estimation. As the temperature inside the arc is very high, thermal decomposition of CO_2 is included in our model through the reactions $CO_2 + M \rightarrow CO + O + M$ and $CO_2 + O \rightarrow CO + O_2$, along with their reverse processes. Our calculations reveal that thermal conversion is responsible for about 90% of the total CO_2 conversion at this high temperature. This maximum is reached faster at lower flow rates (i.e., even at 0.5 cm for 10 L/min), which is logical, as the gas has more time to be heated. The vibrational temperature (Figure 2b) and electron density (Figure 2d) follow the same trend, achieving their maximum values (~3340 K and 8.5×10^{11} cm^{-3}, respectively) at the same positions. We were not able to compare the electron density with experimental values, and we are not aware of such measurements in a CO_2 GAP. In a conventional gliding arc, the electron density in air was measured to be 10^{12}−10^{13} cm^{-3}.[50] However, CO_2 has more internal degrees of freedom than N_2 and O_2, so we expect less electron energy to go to ionization and more to go toward vibrational excitation, which can explain the lower electron density than in air. The fact that our calculated values are rather low can be attributed to the 0D approach, which does not capture nonuniformity in the arc discharge, such as higher power density in the center, which can lead to higher electron densities. However, according to ref 22, the GAP operates in the transitional regime where the electron density lies typically between 10^{11} and 10^{12} cm^{-3}, so we think that our values are reasonable."

The initial electron temperature (Figure 2c) is equal to 2.3 eV, and it decreases to 1.1 eV when the maximum gas temperature is reached. This higher electron temperature in the beginning of the arc can be attributed to the fact that the power is initially deposited over a small number of electrons. The values obtained for the gas and electron temperatures are typical for the GAP and other types of so-called warm plasmas.[22,24,38]

The electron temperature is much higher than the gas temperature (1.1 eV or 12800 K versus 3340 K), and thus, the plasma is in nonequilibrium, which is most suitable for activating the gas through electron-impact dissociation, ionization, and excitation and, thus, for energy-efficient CO_2 conversion.

Initially, the vibrational temperature is about 2 times higher than the gas temperature, indicating that the vibrational levels are overpopulated and show a nonthermal vibrational distribution function (VDF) (see Figure S.1 of the Supporting Information). The vibrational temperature also exhibits a sharp increase, demonstrating the importance of vibrational excitation in a GAP, as also stated in.[21] However, the sharp increase in vibrational temperature happens at the same position as the increase in gas temperature, and the two temperatures become almost equal to each other, which means that the vibrational levels will become thermalized after a traveled distance greater than 0.60 cm, and they will exhibit a near-Boltzmann distribution (see Figure S.1 of the Supporting Information). Therefore, the highest vibrational levels will not be overpopulated, which would be needed for the most energy-efficient vibration-induced dissociation from the highest levels (see below).

Figure 3 shows the evolution of the CO_2 conversion inside the arc, as a function of position in the arc column, for different flow rates and a plasma power of 650 W. The conversion starts to increase when the vibrational and gas temperatures reach their maximum values. This indicates that vibration-induced dissociation plays a significant role (see also sections 3.3 and 3.4).

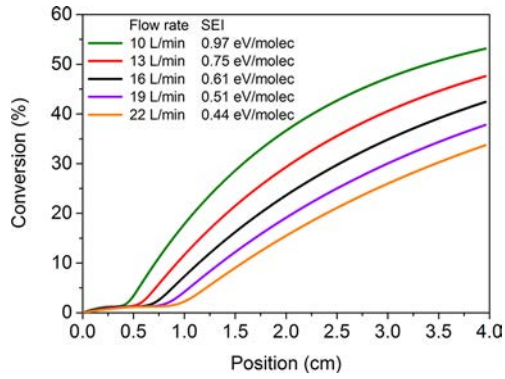

Figure 3. Calculated CO_2 conversion inside the arc as a function of position in the arc column for different gas flow rates at a plasma power of 650 W. The corresponding values of specific energy input (SEI), calculated from the plasma power and gas flow rate (see eq 10), are also indicated.

The conversion is higher at lower flow rates, which is again logical, because the gas has more time to be converted. At 22 L/min, the conversion rises more or less linearly, reaching 35% at the end of the arc column. At 10 L/min, the conversion reaches more than 50% at the end of the arc column, but after a linear increase up to 1.5 cm, the rise becomes less significant, indicating that the reverse reaction (i.e., recombination of CO into CO_2) becomes important as soon as about 30% of the CO_2 molecules are converted (see also section 3.3 below).

3.2. Overall CO_2 Conversion and Energy Efficiency. The overall CO_2 conversion will be lower than the values

DOI: 10.1021/acs.jpcc.7b06524
J. Phys. Chem. C 2017, 121, 22644−22655

obtained inside the arc, as a significant fraction of the gas (i.e., about 85%) does not pass through the arc column and will not be converted. Thus, the CO_2 conversion at the end of the arc column must be multiplied by 14.8% to obtain the overall CO_2 conversion, as explained in detail in section 2.3 above. The overall CO_2 conversion is depicted in Figure 4 as a function of

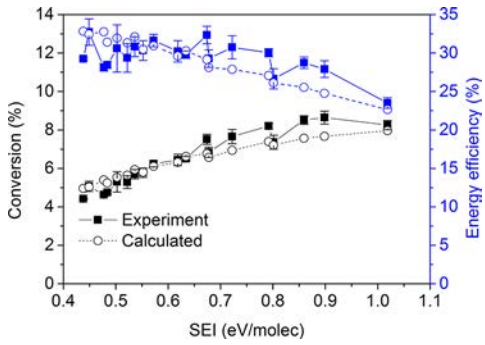

Figure 4. Calculated and measured CO_2 conversions (left axis) and corresponding energy efficiencies (right axis) as functions of the specific energy input (SEI), which is a combination of different values of the gas flow rate and plasma power. The experimental data were obtained from ref 23.

SEI, together with the experimentally obtained conversions and the energy efficiencies (calculated with eqs 5, 9, and 10 of section 2.3), for the conditions studied in ref 23, namely, different combinations of gas flow rate and plasma power. It is clear that the overall conversion is more limited, having a maximum of about 8%. The calculated conversions and energy efficiencies show good agreement with the experimental results, with an average relative error of 6% and a maximum relative error of 16% at SEI = 0.48 eV/molecule.

Both the model and the simulations indicate energy efficiencies up to 33% for a CO_2 conversion of 7.5%. Similar values of conversion between 2% and 9% and energy efficiencies between 22% and 37% were achieved in the GAP of ref 21. Furthermore, in an ac-pulsed reverse vortex "tornado" flow GA plasma,[25] a CO_2 conversion of 6% with a corresponding energy efficiency of 29% was obtained, again very similar to our results. These energy efficiencies are somewhat higher than for earlier experiments with conventional GA plasmas, for which maximum energy efficiencies of approximately 25% were reported,[18] but at higher conversions of 18%. In a recent study of a conventional GA,[20] conversions in the range of 6−10% were found with energy efficiencies between 20% and 40%, which is comparable to and even slightly better than our results. However, in that case, the GA was sealed in an insulated container, providing for recirculation of the gas through the arc, so that a larger fraction of the gas could be treated.

Snoeckx and Bogaerts recently reported a very detailed comparison of the CO_2 conversions and energy efficiencies in all types of plasmas that have been investigated so far,[4] which showed that the GAP is among the most energy-efficient plasma sources for CO_2 conversion. The highest energy efficiencies ever measured were in a microwave (MW) discharge with values up until 60%[14,51] and even 80−90%.[13,16] However, the latter results were obtained using supersonic flows combined with reduced pressure, conditions that are undesirable for upscaling to an industrial scale. Furthermore, when MW plasmas operate at atmospheric pressure, the energy efficiency typically drops to 5−20%.[17] One of the most suitable reactors for upscaling is the dielectric barrier discharge (DBD) reactor, because of its robust design and atmospheric-pressure operation. However, the energy efficiency is generally (much) lower than in a GA, with values typically reported up to a maximum of 10−15%, although, recently, energy efficiencies up until 23% were achieved for a CO_2 conversion of 26% in a DBD in burst mode.[6]

Although the GAP thus shows promising results, also in comparison with other plasma types, the conversion and energy efficiency should still be improved for further exploitation. As there is very good agreement between the calculated and experimental conversions and energy efficiencies, we conclude that the model used in this work provides a realistic picture of the CO_2 conversion and that it can thus be used to elucidate the underlying reaction pathways, which is needed to further improve the performance. This task is discussed in the next section.

3.3. Chemical Pathway Analysis of CO_2 Conversion. In Figure 5, we plot the rates, integrated over the entire residence time of the gas inside the plasma, of the most important loss and formation processes of CO_2 as functions of the SEI. The total time-integrated rate of the loss processes is only a factor of about 2−3 higher than the total time-integrated rate of the formation processes, namely, $(1.0-2.5) \times 10^{18}$ cm^{-3} versus $(0.23-1.3) \times 10^{18}$ cm^{-3}, for all conditions investigated. This indicates that a significant fraction of the dissociated CO_2 (in the form of CO, O, and O_2) will recombine again inside the plasma. Indeed, the reaction products of the dissociation processes are also the most important reactants for the formation of CO_2, as explained below.

It is clear from Figure 5a that vibration-induced dissociation plays a significant role in converting CO_2. The most important dissociation processes are the collisions of vibrationally excited CO_2 with an O atom, forming CO and O_2, followed by the collision with any neutral species (denoted as M), forming CO and O. Electron-impact dissociation from the ground state and from the vibrationally excited states of CO_2 also plays a role, but the rates of these processes are about 3 times lower.

The most important mechanism of CO_2 formation (see Figure 5b) is the reaction between CO and O_2, re-forming CO_2 and an O atom, followed by the three-body recombination ($CO + O + M \rightarrow CO_2 + M$), although the rate of the latter process is almost 1 order of magnitude lower.

Because the most important formation processes are the reverse of the most important loss processes, one must look at the net rates of these processes (i.e., loss minus formation), depicted in Figure 5c. It is clear that dissociation upon collision with an O atom and dissociation upon collision with any neutral species M, primarily from vibrationally excited CO_2, contribute almost equally toward the CO_2 dissociation, with relative contributions of 38% and 40% at the lowest and highest SEI values, respectively. These processes are followed by electron-impact dissociation from the ground state (14% and 10% at the lowest and highest SEI values) and from vibrationally excited CO_2 (~7%, independent of the SEI).

A general reaction scheme illustrating the main pathways of CO_2 dissociation in the GAP is presented in Figure 6. The process is initiated by electron-impact excitation from the CO_2 ground state, populating the vibrational levels (black arrows). Furthermore, molecules in the lowest vibrational levels $[CO_2(v_i)]$ collide with each other, gradually populating the higher vibrational levels $[CO_2(v_{j>i})]$ through so-called VV

DOI: 10.1021/acs.jpcc.7b06524
J. Phys. Chem. C 2017, 121, 22644−22655

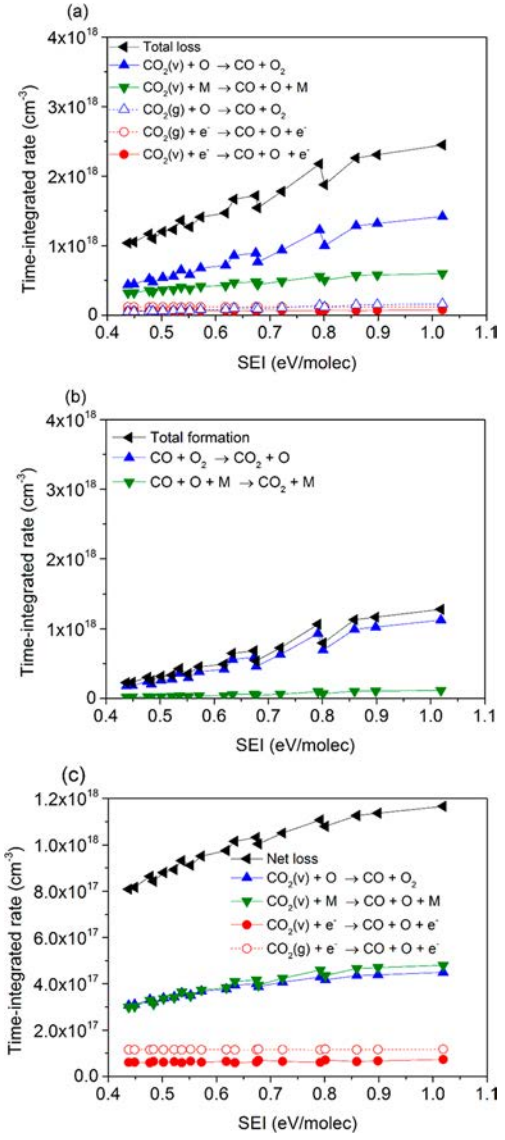

Figure 5. Time-integrated rates of the main (a) loss and (b) formation mechanisms of CO_2 and of the (c) main net loss mechanisms as functions of the specific energy input (SEI). The same colors are used in all three panels for the same processes. Solid lines/solid symbols denote the processes from the vibrational levels, whereas dashed lines/open symbols apply to the processes from the ground state.

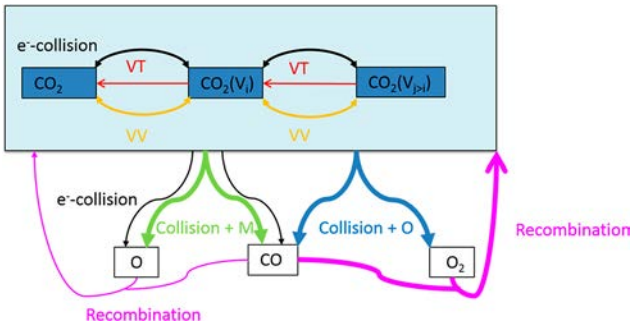

Figure 6. Reaction scheme illustrating the main pathways for CO_2 conversion in the GAP.

relaxation (yellow arrows). At the same time, molecules in different vibrational levels also collide with neutral species in so-called VT relaxation (red arrows), which leads to loss of the higher levels and thermalization of the VDF. VV relaxation is thus generally beneficial for energy-efficient CO_2 conversion, whereas VT relaxation has a negative effect. The dissociation of CO_2 occurs upon collision with O atoms (blue arrows), any neutral species M (green arrows), and electrons (black arrows), mainly from the CO_2 vibrational levels, although electron-impact dissociation mainly occurs from the ground state (see Figure 5). At the same time, recombination of CO with O or O_2 also takes place, re-forming CO_2 (purple arrows), which should be avoided.

3.4. Role of the Vibrational Levels in CO_2 Dissociation.

It is clear from Figure 5 that most of the CO_2 dissociation occurs from the vibrational levels. To understand which vibrational levels contribute most, we plot in Figure 7 the net

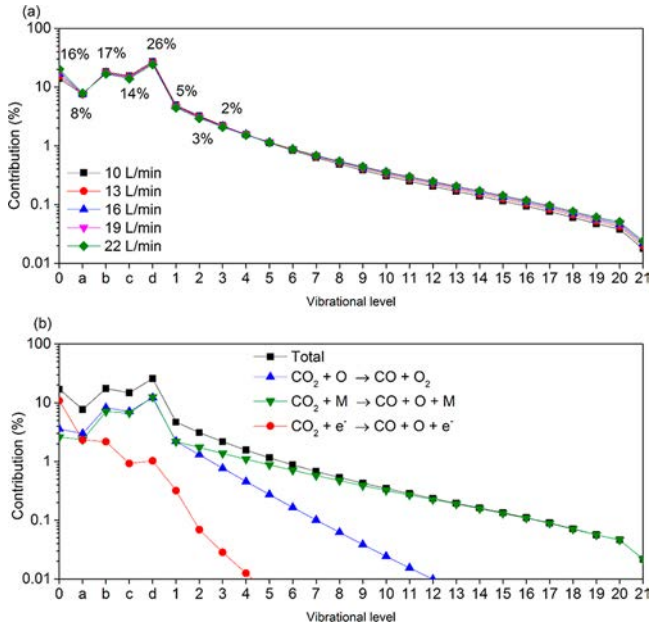

Figure 7. (a) Relative contributions of the different vibrational levels of CO_2 to the total dissociation of CO_2 for different flow rates at an input power of 650 W and (b) contributions of the individual processes for each vibrational level at a flow rate of 16 L/min and an input power of 650 W.

contributions of the different vibrational levels to the dissociation of CO_2 at 650 W for different flow rates, as well as the main dissociation processes occurring at each vibrational level at a flow rate of 16 L/min. As shown in Figure 7a, for all flow rates studied, most dissociation occurs from the symmetric-mode vibrational levels (i.e., combined levels Va–Vd, as identified in Table S.1 of the Supporting Information; overall contribution of ~65%), followed by the ground state (contribution of ~16%) and the first three asymmetric-mode vibrational levels (overall contribution of ~10%). The remaining 9% of the CO_2 dissociation arises from the higher asymmetric-mode levels. This low contribution is due to the fact that the vibrational distribution function (VDF) quickly becomes quasi-Boltzmann distributed at positions of >0.60 cm (see Figure S.1 of the Supporting Information). This means that the highest levels will not be overpopulated, as is the case, for instance, in MW plasmas at reduced pressure.[11,15,34] Therefore, dissociation will occur from the lowest levels instead of from the more desirable highest levels. Indeed, at

DOI: 10.1021/acs.jpcc.7b06524
J. Phys. Chem. C 2017, 121, 22644–22655

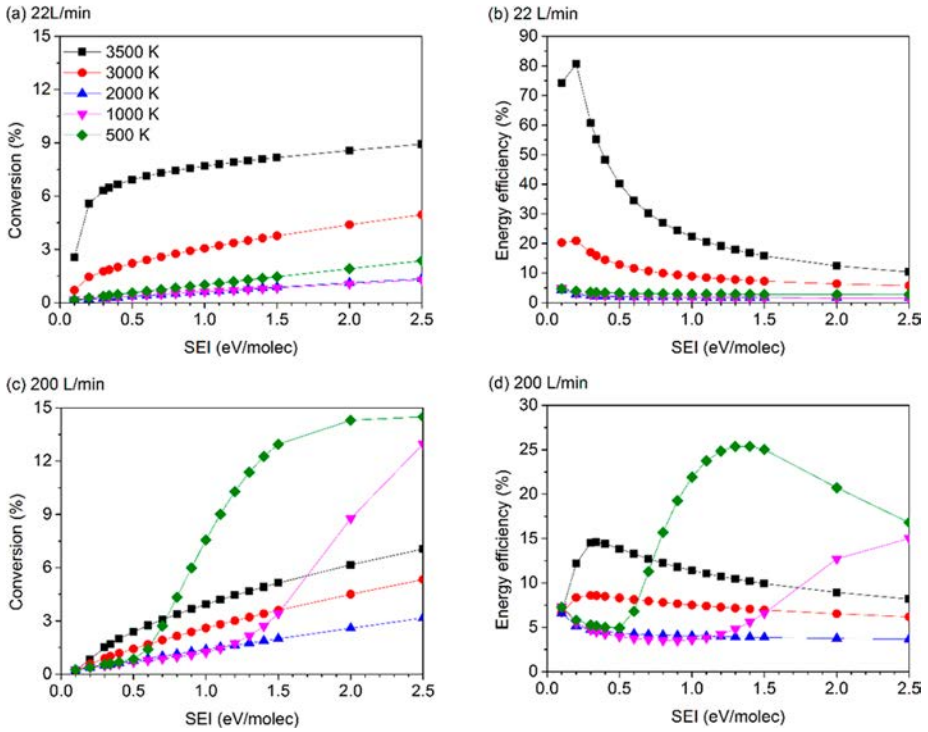

Figure 8. (a,c) CO_2 conversion and (b,d) energy efficiency as functions of SEI for different maximum gas temperatures in the arc column at flow rates of (a,b) 22 and (c,d) 200 L/min. The plasma power values needed to reach this SEI range vary between 147 W and 3.68 kW for 22 L/min and between 1.34 and 33.4 kW for 200 L/min.

atmospheric pressure and high gas temperatures, VT relaxation will play an important role in thermalizing the VDF. The same was observed in refs 15 and 16 for a MW discharge at atmospheric pressure.

Figure 7b demonstrates that the vibration-induced dissociation of the symmetric-mode levels, upon collision with an O atom or a neutral species M, contributes most to the dissociation of CO_2, whereas electron-impact dissociation mainly occurs from the CO_2 ground state. This process, as well as collision with an O atom, becomes less important with increasing asymmetric-mode level. Indeed, for these higher levels, dissociation upon collision with any neutral species M is the most important. Because most dissociation occurs from the lowest levels, we do not further discuss the dissociation kinetics from the higher asymmetric-mode levels.

3.5. Optimizing the CO_2 Conversion and Energy Efficiency. Although the GAP already performs quite well compared to other plasma types,[4] it is clear that there is still room for improvement, if the role of higher vibrational levels could be better exploited or the rate of CO_2 formation could be reduced. Zero-dimensional kinetic modeling allows for the study of the effects of different plasma conditions, beyond what is experimentally feasible, on the CO_2 chemistry and, thus, on the CO_2 conversion and energy efficiency, to provide conceptual information about how to improve the GAP. In the following subsections, we study the effects of (i) lowering and increasing the gas temperature, as this affects the VDF,[15] and (ii) removing the O_2 molecules to block the main formation process of CO_2. We also extend the range of SEI values from 0.1 to 2.5 eV/molecule, so we investigate a wide range of powers (between 147 W and 33.4 kW) and gas flow rates (between 22 and 200 L/min). It should be realized that some combinations, such as high SEI values and low gas temperatures, cannot yet be experimentally achieved, but the modeling results might provide valuable insights for future reactor design. The flow rates used in the following subsections are 22 and 200 L/min. Indeed, the highest energy efficiency in our experiments was obtained for 22 L/min,[23] whereas flow rates of about 200 L/min were applied in ref 52, where a high-power GAP was designed for upscaling toward industrial applications.

The predicted conversions and energy efficiencies as functions of flow rate between 22 and 200 L/min and for different values of the SEI are plotted in Figures S.2 and S.3 of the Supporting Information for maximum gas temperatures of 500 and 3500 K, respectively. Gradual changes are observed in both conversion and energy efficiency between the values obtained at 22 and 200 L/min. Therefore, in the following discussion, we show the results only for the minimum and maximum flow rates.

3.5.1. Influence of the Gas Temperature. As mentioned above, a high gas temperature enhances VT relaxation, which has a negative effect on energy-efficient CO_2 conversion because it depopulates the higher vibrational levels. On the other hand, the rates of the dissociation reactions upon collision with O atoms or any neutral species M also rise with temperature. Therefore, it is important to investigate the effects of the maximum gas temperature in the arc column on the CO_2 conversion and energy efficiency. The results are shown as functions of SEI in Figure 8 for flow rates of 22 and 200 L/min. In both cases, we vary the SEI between 0.1 and 2.5 eV/molecule. This corresponds to plasma powers between 147 W and 3.68 kW for the flow rate of 22 L/min and values between 1.34 and 33.4 kW for the flow rate of 200 L/min.

At 22 L/min (Figure 8a,b), the power seems to be too low for sufficient electron-impact vibrational excitation followed by vibrational pumping toward the highest levels, and thus for dissociation from these highest levels, at all SEI values studied.

DOI: 10.1021/acs.jpcc.7b06524
J. Phys. Chem. C 2017, 121, 22644−22655

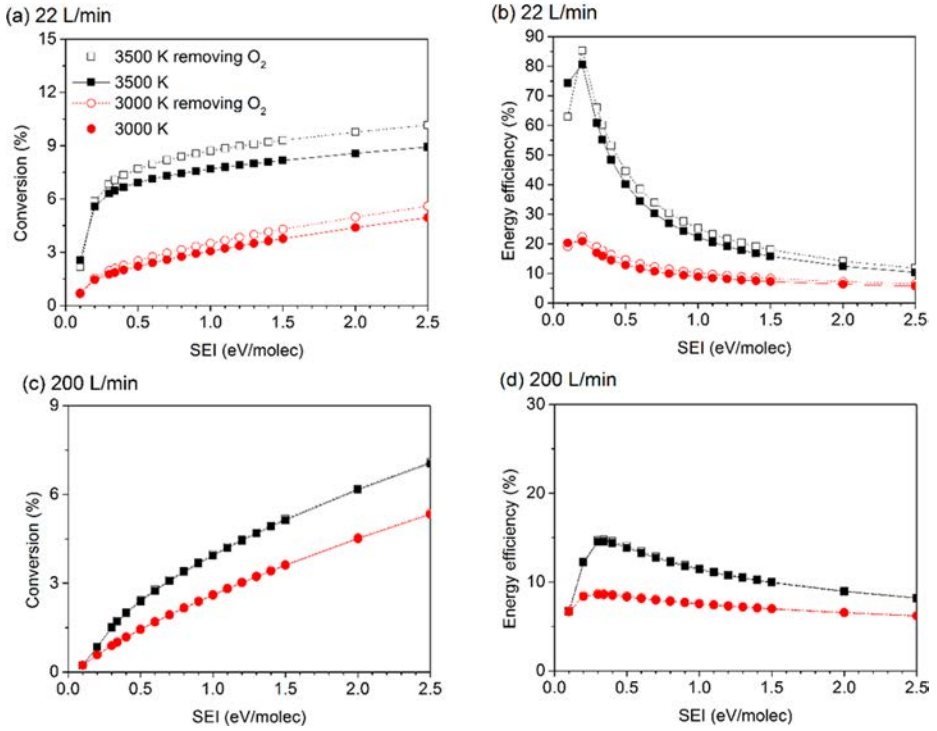

Figure 9. (a,c) CO_2 conversion and (b,d) energy efficiency as functions of SEI for (a,b) 22 and (c,d) 200 L/min when the O_2 molecules are artificially removed from the system (dashed lines, open symbols) or not (solid lines, solid symbols).

At the low gas temperature of 500 K, where VT relaxation is suppressed, our calculations predict that dissociation upon collision with neutral species does not contribute at all to CO_2 dissociation and that dissociation is almost entirely by electron-impact dissociation from the ground state and the lowest vibrational levels. This is true for the entire range of SEI values (see Figures S.4a and S.5a of the Supporting Information for SEI values of 2.5 and 0.2 eV/molecule, respectively). Especially at low SEI values, electron-impact dissociation mainly occurs from the ground state (see Figure S.5a). This process is less energy-efficient than dissociation from the vibrational levels upon collision with neutral species. Thus, the CO_2 conversion and energy efficiency will rise with increasing gas temperature for 22 L/min, as is obvious from Figure 8a,b, because dissociation upon collision with neutral species (either O atoms or any molecule M) from the (low) vibrational levels becomes increasingly important at the higher gas temperature (cf. Figures S.4b and S.5b of the Supporting Information, where these processes are shown to be dominant for a gas temperature of 3500 K and SEI values of 2.5 and 0.2 eV/molecule, respectively).

As illustrated in Figure 8a,b, at this flow rate of 22 L/min, a maximum conversion of 9% is obtained at 3500 K and an SEI of 2.5 eV/molecule, but it corresponds to a low energy efficiency of 10%, whereas a maximum energy efficiency of greater than 80% is predicted at the same temperature but at an SEI of 0.2 eV/molecule, corresponding to a low conversion of 6%. It should be noted, however, that, in reality, temperatures of 3500 K are highly unlikely at SEI values less than 0.34 eV/molecule and, thus, an external heat source would be necessary to achieve this temperature. This would yield a higher overall SEI and thus lower energy efficiencies.

At a flow rate of 200 L/min (Figure 8c,d, the CO_2 conversion and energy efficiency follow the same trend as at 22 L/min for SEI values below 0.7 eV/molecule, with rising conversion and energy efficiency at higher temperatures. The maximum energy efficiency in this range was calculated to be 15%, at an SEI of 0.34 eV/molecule and 3500 K. In this case, dissociation upon collision with O atoms or molecules M also plays a significant role, although it is less significant than at 22 L/min, because of the higher plasma power for the same SEI and, thus, the larger contribution of electron-impact dissociation (see Figure S.6 of the Supporting Information). As the latter process is less energy-efficient than dissociation upon collision with neutral species, this explains the lower energy efficiency.

For SEI values greater than 0.7 eV/molecule, the behavior at 200 L/min is different from that at 22 L/min. Indeed, the conversion and energy efficiency rise as the gas temperature is decreased to 1000 K and especially 500 K (see Figure 8c,d). The reason is that vibrational excitation followed by vibrational pumping, and hence vibration-induced dissociation from the highest levels, now becomes dominant, as can be deduced from Figure S.7a of the Supporting Information. Indeed, the contribution of vibration-induced dissociation from the highest vibrational levels, which is the most desired way of dissociating CO_2, is 81% in this case. However, this situation is reached only at very high plasma powers, to obtain these high SEI values (above 0.7−1 eV/molecule) at the flow rate of 200 L/min, and thus the energy efficiency (maximum 25%) is still lower than the values that we obtained in our experiments,[23] but the corresponding conversion is somewhat higher (ca. 12%) than our best values.[23] At higher gas temperatures, the CO_2 conversion and energy efficiency drop as a result of thermalization of the VDF, until 3000 K, where they again rise because of the increasing importance of dissociation upon collision with the neutral species (see also Figure S.7b,c of the Supporting Information).

DOI: 10.1021/acs.jpcc.7b06524
J. Phys. Chem. C 2017, 121, 22644−22655

We thus conclude that, for low flow rates (e.g., 22 L/min), a higher gas temperature leads to a higher conversion and energy efficiency, which is attributed to thermal dissociation. This is true at all SEI values (and thus powers) investigated, but the energy efficiency is a maximum at low SEI. On the other hand, at high flow rates and sufficiently high SEI values (and thus very high power values), electron-impact vibrational excitation followed by pumping, and thus vibration-induced dissociation from the highest levels, becomes much more significant at lower gas temperatures, because of the decrease in VT relaxation, and therefore, under these conditions, lower gas temperatures lead to higher conversion and energy efficiency.

3.5.2. Removing the O_2 Molecules. As shown in Figure 5, the total rate of CO_2 formation is only 2−3 times lower than the total rate of CO_2 loss, and this is mainly due to the recombination of CO with O_2 molecules. Hence, we used the model to determine whether removing the O_2 molecules from the system can improve the overall CO_2 conversion. Methods to realize this could be centrifugation, distillation, and absorption, but such methods are difficult and not energy-efficient, because of the small difference in the molar masses of CO and O_2.[53,54] Nevertheless, we investigated this effect theoretically, because novel and more energy-efficient methods might be developed in the future. The effects of removing the O_2 molecules from the system on the CO_2 conversion and energy efficiency are presented in Figure 9 for flow rates of 22 and 200 L/min and typical maximum arc temperatures of 3000 and 3500 K.

At a flow rate of 22 L/min, O_2 removal has a slightly positive effect on the CO_2 conversion and energy efficiency at both temperatures investigated (see Figure 9a,b). The reason the effect is so small is as follows: When O_2 is removed, the CO_2 formation process due to recombination of CO with O_2 ($CO + O_2 \rightarrow CO_2 + O$) is indeed zero, but this also means that no O atoms can be formed by this process. Furthermore, no O atoms can be formed by the dissociation of O_2 either. Hence, the O-atom density drops significantly, and dissociation upon collision of vibrationally excited CO_2 with O atoms also drops. Thus, not only does CO_2 formation decrease, but CO_2 loss decreases as well. Therefore, the net positive effect of O_2 removal on the CO_2 conversion and energy efficiency is very small. At 200 L/min, the effect of O_2 removal is even completely negligible (see Figure 9c,d).

To realize a higher CO_2 conversion, it would thus be necessary to remove the O_2 molecules but, at the same time, to leave the O-atom production undisturbed or (more realistically) to replace O atoms by another active agent that can contribute to CO_2 dissociation, such as H atoms. Adding a hydrogen source such as CH_4 or H_2 might thus provide a solution. Indeed, combined CO_2/CH_4 conversion (or dry reforming of methane)[25] and CO_2/H_2 conversion[21] typically yield higher CO_2 conversions and energy efficiencies.

4. CONCLUSIONS

We have presented a chemical kinetics study to elucidate the main dissociation mechanisms of CO_2 in a GAP, with special emphasis on the role of the vibrational kinetics. The CO_2 conversions and energy efficiencies calculated with the model for a wide range of SEI values (corresponding to different values of power and gas flow rate) are in good agreement with experimental values obtained under the same conditions. This agreement indicates that the model can provide a realistic picture of CO_2 conversion in the GAP and can thus be used to identify its limitations and propose solutions for further improvement.

The results obtained, both experimentally and with the model, demonstrate that the GAP is promising for CO_2 conversion, with energy efficiencies ranging between 23% and 33%. This is explained by the large contribution of dissociation of the vibrationally excited levels upon collision with an O atom ($CO_2 + O \rightarrow CO + O_2$) or any neutral species M ($CO_2 + M \rightarrow CO + O + M$). However, because of the high gas temperature in the GAP, the VDF exhibits a quasi-Boltzmann distribution with low population of the highest vibrational levels. Therefore, the dissociation mainly occurs from the lowest symmetric-mode levels (contribution of ∼65%), followed by the ground state (contribution of ∼16%) and the first three asymmetric-mode levels (contribution of ∼10%), whereas the higher asymmetric-mode levels have a negligible contribution.

A more pronounced overpopulation of the highest asymmetric-mode levels, and thus dissociation from these levels, would further increase the energy efficiency. This overpopulation can, in principle, be achieved at lower gas temperatures, because lower temperatures reduce the VT relaxation. On the other hand, lower temperatures also result in lower dissociation rates of the CO_2 vibrational levels upon collision with O atoms or neutral molecules M. Thus, our calculations reveal that, in general, lowering the gas temperature has no positive effect on the CO_2 conversion and energy efficiency. Only at 200 L/min and SEI values greater than 0.7 eV/molecule does a gas temperature of 500 K yield better results than higher temperatures, because the dissociation mainly occurs from the highest asymmetric-mode vibrational levels. However, this energy-efficient dissociation mechanism cannot compensate for the large amount of power needed to induce it (>9.4 kW), and the maximum energy efficiency obtained is still limited to 25%, although the conversion is slightly enhanced.

Furthermore, our calculations reveal that the recombination reaction ($CO + O_2 \rightarrow CO_2 + O$) is the main factor limiting the overall CO_2 conversion, because a large fraction of the dissociated CO_2 (in the form of CO, O, and O_2) will recombine again into CO_2. Therefore, we also performed simulations in which the O_2 molecules were removed from the system. However, this has only a minor positive effect on the conversion and energy efficiency, because the O-atom production by this process and by the dissociation of O_2 is also inhibited, and these O atoms are needed to react with vibrationally excited CO_2 molecules to provide more dissociation.

It is clear that the chemistry of CO_2 dissociation in a GAP is quite complicated, and simply reducing the gas temperature or removing the O_2 molecules from the system does not yield significantly better results than those already obtained experimentally. We believe that, to further improve the performance of the GAP, one should target a higher fraction of gas that can be converted by the plasma column, because the latter is now limited to about 15%. This effect cannot be studied by 0D modeling, but rather, 3D fluid dynamics simulations would be needed for this purpose.[23,24,38] Finally, mixing the CO_2 gas with a hydrogen source, such as H_2 or CH_4, might also improve the CO_2 conversion, as the H atoms can contribute to CO_2 dissociation. This approach will be investigated in our future research.

DOI: 10.1021/acs.jpcc.7b06524
J. Phys. Chem. C 2017, 121, 22644−22655

■ ASSOCIATED CONTENT

Supporting Information

The Supporting Information is available free of charge on the ACS Publications website at DOI: 10.1021/acs.jpcc.7b06524.

More detailed description of the 0D model, together with an explanation of the notation of the different vibrational levels implemented in the chemistry data set; calculated vibrational distribution functions at different positions in the arc column for a plasma power of 650 W and flow rates of 10 and 22 L/min; effects of the flow rate on the CO_2 conversion and energy efficiency for maximum gas temperatures of 500 and 3500 K at different SEI values; and contributions of the different vibrational levels to CO_2 dissociation for different conditions (PDF)

■ AUTHOR INFORMATION

Corresponding Author

*E-mail: annemie.bogaerts@uantwerpen.be. Phone: +3232652377.

ORCID

Stijn Heijkers: 0000-0001-7142-9697

Notes

The authors declare no competing financial interest.

■ ACKNOWLEDGMENTS

The authors acknowledge financial support from the Fund for Scientific Research − Flanders (FWO; Grant G.0383.16N) and the IAP/7 (Interuniversity Attraction Pole) program 'PSI-Physical Chemistry of Plasma-Surface Interactions' by the Belgian Federal Office for Science Policy (BELSPO). The calculations were performed using the Turing HPC infrastructure at the CalcUA core facility of Universiteit Antwerpen, a division of the Flemish Supercomputer Center VSC, funded by the Hercules Foundation, the Flemish Government (department EWI), and Universiteit Antwerpen. Finally, the authors thank Marleen Ramakers and Georgi Trenchev for providing the experimental data and the 3D fluid modeling results, respectively, as input data for the model.

■ REFERENCES

(1) Blunden, J.; Arndt, D. S. State of the Climate in 2015. *Bull. Am. Meteorol. Soc.* **2016**, *97* (8), S1−S275.

(2) *Report of the Conference of the Parties on Its Twenty-First Session, Held in Paris from 30 November to 13 December 2015*; Report FCCC/CP/2015/10; United Nations Framework Convention on Climate Change: Paris, 2015.

(3) McDonough, W.; Braungart, M.; Anastas, P. T.; Zimmerman, J. B. Peer Reviewed: Applying the Principles of Green Engineering to Cradle-to-Cradle Design. *Environ. Sci. Technol.* **2003**, *37* (23), 434A−441A.

(4) Snoeckx, R.; Bogaerts, A. Plasma Technology − a Novel Solution for CO_2 Conversion? *Chem. Soc. Rev.* [Advance Article]. DOI: 10.1039/C6CS00066E. Published Online: Aug 21, 2017. http://pubs.rsc.org/en/content/articlelanding/2017/cs/c6cs00066e.

(5) Aerts, R.; Somers, W.; Bogaerts, A. Carbon Dioxide Splitting in a Dielectric Barrier Discharge Plasma: A Combined Experimental and Computational Study. *ChemSusChem* **2015**, *8* (4), 702−716.

(6) Ozkan, A.; Dufour, T.; Silva, T.; Britun, N.; Snyders, R.; Reniers, F.; Bogaerts, A. DBD in Burst Mode: Solution for More Efficient CO_2 Conversion ? *Plasma Sources Sci. Technol.* **2016**, *25* (5), 055005.

(7) Paulussen, S.; Verheyde, B.; Tu, X.; De Bie, C.; Martens, T.; Petrovic, D.; Bogaerts, A.; Sels, B. Conversion of Carbon Dioxide to Value-Added Chemicals in Atmospheric Pressure Dielectric Barrier Discharges. *Plasma Sources Sci. Technol.* **2010**, *19*, 034015.

(8) Silva, T.; Britun, N.; Godfroid, T.; Snyders, R. Optical Characterization of a Microwave Pulsed Discharge Used for Dissociation of CO_2. *Plasma Sources Sci. Technol.* **2014**, *23*, 025009.

(9) Kwak, H. S.; Uhm, H. S.; Hong, Y. C.; Choi, E. H. Disintegration of Carbon Dioxide Molecules in a Microwave Plasma Torch. *Sci. Rep.* **2016**, *5*, 18436.

(10) van Rooij, G. J.; van den Bekerom, D. C. M.; den Harder, N.; Minea, T.; Berden, G.; Bongers, W. A.; Engeln, R.; Graswinckel, M. F.; Zoethout, E.; van de Sanden, M. C. M. Taming Microwave Plasma to Beat Thermodynamics in CO_2 Dissociation. *Faraday Discuss.* **2015**, *183*, 233−248.

(11) Kozák, T.; Bogaerts, A. Splitting of CO_2 by Vibrational Excitation in Non-Equilibrium Plasmas: A Reaction Kinetics Model. *Plasma Sources Sci. Technol.* **2014**, *23*, 045004.

(12) Kozák, T.; Bogaerts, A. Evaluation of the Energy Efficiency of CO_2 Conversion in Microwave Discharges Using a Reaction Kinetics Model. *Plasma Sources Sci. Technol.* **2015**, *24*, 015024.

(13) Asisov, R. I.; Givotov, V. K.; Krasheninnikov, E. G.; Potapkin, B. V.; Rusanov, V. D.; Fridman, A. Carbon Dioxide Dissociation in Non-Equilibrium Plasma. *Sov. Phys. Dokl.* **1983**, *271*, 94.

(14) Bongers, W.; Bouwmeester, H.; Wolf, B.; Peeters, F.; Welzel, S.; van den Bekerom, D.; den Harder, N.; Goede, A.; Graswinckel, M.; Groen, P. W.; et al. Plasma-Driven Dissociation of CO_2 for Fuel Synthesis. *Plasma Processes Polym.* **2017**, *14*, 1600126.

(15) Berthelot, A.; Bogaerts, A. Modeling of CO_2 Splitting in a Microwave Plasma: How to Improve the Conversion and Energy Efficiency. *J. Phys. Chem. C* **2017**, *121* (15), 8236−8251.

(16) Fridman, A. A. *Plasma Chemistry*; Cambridge University Press: New York, 2008.

(17) Spencer, L. F.; Gallimore, A. D. Efficiency of CO_2 Dissociation in a Radio-Frequency Discharge. *Plasma Chem. Plasma Process.* **2011**, *31* (1), 79−89.

(18) Indarto, A.; Yang, D. R.; Choi, J. W.; Lee, H.; Song, H. K. Gliding Arc Plasma Processing of CO_2 Conversion. *J. Hazard. Mater.* **2007**, *146*, 309−315.

(19) Indarto, A.; Choi, J.-W.; Lee, H.; Song, H. K. Conversion of CO_2 by Gliding Arc Plasma. *Environ. Eng. Sci.* **2006**, *23* (6), 1033−1043.

(20) Sun, S. R.; Wang, H. X.; Mei, D. H.; Tu, X.; Bogaerts, A. CO_2 Conversion in a Gliding Arc Plasma: Performance Improvement Based on Chemical Reaction Modeling. *J. CO2 Util.* **2017**, *17*, 220−234.

(21) Nunnally, T.; Gutsol, K.; Rabinovich, A.; Fridman, A.; Gutsol, A.; Kemoun, A. Dissociation of CO_2 in a Low Current Gliding Arc Plasmatron. *J. Phys. D: Appl. Phys.* **2011**, *44*, 274009.

(22) Nunnally, T. P. Application of Low Current Gliding Arc Plasma Discharges for Hydrogen Sulfide Decomposition and Carbon Dioxide Emission Reduction. Ph.D. Dissertation, Drexel University, Philadelphia, PA, 2011.

(23) Ramakers, M.; Trenchev, G.; Heijkers, S.; Wang, W.; Bogaerts, A. Gliding Arc Plasmatron: Providing a Novel Method for Carbon Dioxide Conversion. *ChemSusChem* **2017**, *10*, 2642−2652.

(24) Trenchev, G.; Kolev, S.; Wang, W.; Ramakers, M.; Bogaerts, A. CO_2 Conversion in a Gliding Arc Plasmatron: Multi-Dimensional Modelling for Improved Efficiency, manuscript submitted.

(25) Liu, J. L.; Park, H. W.; Chung, W. J.; Park, D. W. High-Efficient Conversion of CO_2 in AC-Pulsed Tornado Gliding Arc Plasma. *Plasma Chem. Plasma Process.* **2016**, *36* (2), 437−449.

(26) Zhang, J. Q.; Yang, Y. J.; Zhang, J. S.; Liu, Q. Study on the Conversion of CH_4 and CO_2 Using a Pulsed Microwave Plasma under Atmospheric Pressure. *Acta Chim. Sin.* **2002**, *60* (11), 1973−1980.

(27) De Bie, C.; Martens, T.; van Dijk, J.; Paulussen, S.; Verheyde, B.; Corthals, S.; Bogaerts, A. Dielectric Barrier Discharges Used for the Conversion of Greenhouse Gases: Modeling the Plasma Chemistry by Fluid Simulations. *Plasma Sources Sci. Technol.* **2011**, *20* (2), 024008.

(28) Tu, X.; Gallon, H. J.; Twigg, M. V.; Gorry, P. A.; Whitehead, J. C. Dry Reforming of Methane over a Ni/Al_2O_3 Catalyst in a Coaxial

DOI: 10.1021/acs.jpcc.7b06524
J. Phys. Chem. C 2017, 121, 22644−22655

Dielectric Barrier Discharge Reactor. *J. Phys. D: Appl. Phys.* **2011**, *44*, 274007.
(29) Wang, Q.; Yan, B. H.; Jin, Y.; Cheng, Y. Dry Reforming of Methane in a Dielectric Barrier Discharge Reactor with Ni/Al_2O_3 Catalyst: Interaction of Catalyst and Plasma. *Plasma Chem. Plasma Process.* **2009**, *29* (18), 217−228.
(30) Snoeckx, R.; Aerts, R.; Tu, X.; Bogaerts, A. Plasma-Based Dry Reforming: A Computational Study Ranging from the Nanoseconds to Seconds Time Scale. *J. Phys. Chem. C* **2013**, *117*, 4957−4970.
(31) Gallon, H. J.; Tu, X.; Whitehead, J. C. Effects of Reactor Packing Materials on H_2 Production by CO_2 Reforming of CH_4 in a Dielectric Barrier Discharge. *Plasma Processes Polym.* **2012**, *9* (1), 90−97.
(32) Snoeckx, R.; Ozkan, A.; Reniers, F.; Bogaerts, A. The Quest for Value-Added Products from Carbon Dioxide and Water in a Dielectric Barrier Discharge: A Chemical Kinetics Study. *ChemSusChem* **2017**, *10* (2), 409−424.
(33) Snoeckx, R.; Heijkers, S.; Van Wesenbeeck, K.; Lenaerts, S.; Bogaerts, A. CO_2 Conversion in a Dielectric Barrier Discharge Plasma: N_2 in the Mix as a Helping Hand or Problematic Impurity? *Energy Environ. Sci.* **2016**, *9*, 999−1011 (15/12/2015 published online).
(34) Heijkers, S.; Snoeckx, R.; Kozák, T.; Silva, T.; Godfroid, T.; Britun, N.; Snyders, R.; Bogaerts, A. CO_2 Conversion in a Microwave Plasma Reactor in the Presence of N_2: Elucidating the Role of Vibrational Levels. *J. Phys. Chem. C* **2015**, *119*, 12815−12828.
(35) Kano, M.; Satoh, G.; Iizuka, S. Reforming of Carbon Dioxide to Methane and Methanol by Electric Impulse Low-Pressure Discharge with Hydrogen. *Plasma Chem. Plasma Process.* **2012**, *32*, 177−185.
(36) Kogelschatz, U. Dielectric-Barrier Discharges: Their History, Discharge Physics, and Industrial Applications. *Plasma Chem. Plasma Process.* **2003**, *23* (1), 1−46.
(37) Kalra, C. S.; Cho, Y. I.; Gutsol, A.; Fridman, A.; Rufael, T. S. Gliding Arc in Tornado Using a Reverse Vortex Flow. *Rev. Sci. Instrum.* **2005**, *76* (2), 025110.
(38) Trenchev, G.; Kolev, S.; Bogaerts, A. A 3D Model of a Reverse Vortex Flow Gliding Arc Reactor. *Plasma Sources Sci. Technol.* **2016**, *25* (3), 035014.
(39) Koelman, P.; Heijkers, S.; Tadayon Mousavi, S.; Graef, W.; Mihailova, D.; Kozák, T.; Bogaerts, A.; van Dijk, J. A Comprehensive Chemical Model for the Splitting of CO_2 in Non-Equilibrium Plasmas. *Plasma Processes Polym.* **2017**, *14*, 1600155.
(40) Plasma Data Exchange Project. www.lxcat.net (accessed 05/03/2017).
(41) Lowke, J. J.; Phelps, A. V.; Irwin, B. W. Predicted Electron Transport Coefficients and Operating Characteristics of $CO_2/N_2/He$ Laser Mixtures. *J. Appl. Phys.* **1973**, *44* (10), 4664−4671.
(42) Hake, R. D.; Phelps, A. V. Momentum-Transfer and Inelastic-Collision Cross Sections for Electrons in O_2, CO, and CO_2. *Phys. Rev.* **1967**, *158* (1), 70−84.
(43) Grofulović, M.; Alves, L. L.; Guerra, V. Electron-Neutral Scattering Cross Sections for CO_2 a Complete and Consistent Set and an Assessment of Dissociation. *J. Phys. D: Appl. Phys.* **2016**, *49*, 395207.
(44) Bogaerts, A.; Wang, W.; Berthelot, A.; Guerra, V. Modeling Plasma-Based CO_2 Conversion: Crucial Role of the Dissociation Cross Section. *Plasma Sources Sci. Technol.* **2016**, *25*, 055016.
(45) Pietanza, L. D.; Colonna, G.; D'Ammando, G.; Laricchiuta, A.; Capitelli, M. Vibrational Excitation and Dissociation Mechanisms of CO_2 under Non-Equilibrium Discharge and Post-Discharge Conditions. *Plasma Sources Sci. Technol.* **2015**, *24* (4), 042002.
(46) Pietanza, L. D.; Colonna, G.; D'Ammando, G.; Laricchiuta, A.; Capitelli, M. Electron Energy Distribution Functions and Fractional Power Transfer in "Cold" and Excited CO_2 Discharge and Post Discharge Conditions. *Phys. Plasmas* **2016**, *23* (1), 013515.
(47) Pietanza, L. D.; Colonna, G.; D'Ammando, G.; Laricchiuta, A.; Capitelli, M. Non Equilibrium Vibrational Assisted Dissociation and Ionization Mechanisms in Cold CO_2 Plasmas. *Chem. Phys.* **2016**, *468*, 44−52.
(48) Snoeckx, R.; Setareh, M.; Aerts, R.; Simon, P.; Maghari, A.; Bogaerts, A. Influence of N_2 Concentration in a CH_4/N_2 Dielectric Barrier Discharge Used for CH_4 Conversion into H_2. *Int. J. Hydrogen Energy* **2013**, *38* (36), 16098−16120.
(49) Menter, F. R.; Kuntz, M.; Langtry, R. Ten Years of Industrial Experience with the SST Turbulence Model. *Turbul., Heat Mass Transfer 4, [Pap. Int. Symp.]* **2003**, *4*, 625−632.
(50) Czernichowski, A.; Nassar, H.; Ranaivosoloarimanana, A.; Fridman, A. A.; Simek, M.; Musiol, K.; Pawelec, E.; Dittrichova, L. Spectral and Electrical Diagnostics of Gliding Arc. *Acta Phys. Pol., A* **1996**, *89* (5-6), 595−603.
(51) Goede, A. P. H.; Bongers, W. A.; Graswinckel, M. G.; van de Sanden, R. M. C. M.; Leins, M.; Kopecki, J.; Schulz, A.; Walker, M. Production of Solar Fuels by CO_2 Plasmolysis. *EPJ Web Conf.* **2014**, *79*, 01005.
(52) Chernets, I.; Nirenberg, G.; Fridman, A.; Rabinovich, A. Development of High-Power Plasma Reformer and Power Supply for Large Scale Applications. Presented at the *20th International Symposium on Plasma Chemistry (ISPC-20)*, Philadelphia, PA, July 24−29, 2011.
(53) Givotov, V. K.; Fridman, A. A.; Krotov, M. F.; Krasheninnikov, E. G.; Patrushev, B. I.; Rusanov, V. D.; Sholin, G. V. Plasmochemical Methods of Hydrogen Production. *Int. J. Hydrogen Energy* **1981**, *6* (5), 441−449.
(54) Aerts, R.; Snoeckx, R.; Bogaerts, A. In-Situ Chemical Trapping of Oxygen in the Splitting of Carbon Dioxide by Plasma. *Plasma Processes Polym.* **2014**, *11*, 985−992.

DOI: 10.1021/acs.jpcc.7b06524
J. Phys. Chem. C 2017, 121, 22644−22655